Materials Today Bio 21 (2023) 100689

Contents lists available at ScienceDirect

Materials Today Bio

journal homepage: www.journals.elsevier.com/materials-today-bio

Accurate imaging in the processes of formation and inhibition of drug-induced liver injury by an activable fluorescent probe for $ONOO^-$

Junming Dong [a], Yushun Yang [b], Xiangjun Fan [c,**], Hai-Liang Zhu [a,***], Zhen Li [a,*]

[a] State Key Laboratory of Pharmaceutical Biotechnology, School of Life Sciences, Nanjing University, No.163 Xianlin Avenue, Nanjing, 210023, China
[b] Jinhua Advanced Research Institute, Jinhua, 321019, China
[c] Department of General Surgery, Affiliated Hospital of Nantong University, Nantong University, 226001, Nantong, China

ARTICLE INFO

Keywords:
Fluorescent probe
Detection of peroxynitrite
Drug-induced liver injury
Accurate real-time imaging

ABSTRACT

Herein, an activable fluorescent probe for peroxynitrite ($ONOO^-$), named **NOP**, was constructed for the accurate imaging in the processes of formation and inhibition of drug-induced liver injury induced by Acetaminophen (APAP). During the in-solution tests on the general optical properties, the probe showed advantages including good stability, wide pH adaption, high specificity and sensitivity in the monitoring of $ONOO^-$. Subsequently, the probe was further applied in the model mice which used APAP to induce the injury and used inhibiting agents (GSH, Glu, NAC) to treat the induced injury. The construction of the liver injury model was confirmed by the pathological staining and the serum indexes including ALT, AST, ALP, TBIL as well as LDH. During the formation of the drug-induced liver injury, the fluorescence in the red channel enhanced in both time-dependent and dose-dependent manners. In inhibition tests, the inhibition of the liver injury exhibited the reduction of the fluorescence intensity. Therefore, **NOP** could achieve the accurate imaging in the processes of formation and inhibition of drug-induced liver injury. The information here might be helpful for the early diagnosis and the screening of potent treating candidates in liver injury cases.

1. Introduction

In human, liver is the main organ for the metabolism of various substances including alcohol, medicine, and chemicals [1,2]. In consideration of the vital role of liver in a wide range of physiological procedures, the liver injury can give rise to the loss of normal functions, which will lead to in severe disorders, or even to death [3,4]. The causes of liver injury were complex, among which alcohol and drugs have been reported as common inducers in both acute and chronic liver injuries [5,6]. In particular, the drug-induced liver injury has become a serious risk for human health, because many drugs, including the ones for treating liver injury, are metabolized through liver. Accordingly, the diagnosis and assessment of drug-induced liver injury seem difficult, which consequently leads to the inefficiency in accurate treatment [7,8]. Present diagnosis of liver injury relies on the level of serum indicators including alanine aminotransferase (ALT), aspartate aminotransferase (AST), alkaline phosphatase (ALP) lactate, total bilirubin (TBIL), and dehydrogenase (LDH) [9,10]. However, the serum indicators cannot achieve the real-time and in situ monitoring. There is an urgent need for finding molecular indexes as alternative references. Therefore, developing more accurate implement to describe the drug-induced liver injury in both processes of formation and inhibition remains an emergency for both the diagnosis and treatment.

During the process of seeking for molecular indexes, reactive oxygen species (ROS) and reactive nitrogen species (RNS) have been reported as potential indicators for monitoring the status of liver-related metabolism [11,12]. Both of them are essential by-products of the reactions in liver, thus are tightly associated with the reduction-oxidation status during the biological events. Among them, peroxynitrite ($ONOO^-$) has been reported as one of the most important biomarkers in liver injury [13,14]. In the models of liver injury induced by various factors, $ONOO^-$ could be used as a practical indicator to reflect the degree of injury [15–17]. The enhanced concentrations of endogenous $ONOO^-$ was caused by the disorder of liver function, and then exhibit hepatocellular death. There might be the difference at quantity or order of magnitude of $ONOO^-$ between the pathological environment and the normal states [18,19]. It

* Corresponding author.
** Corresponding author.
*** Corresponding author.
E-mail addresses: zhuhl@nju.edu.cn (H.-L. Zhu), lizhenzfx@nju.edu.cn (Z. Li).

https://doi.org/10.1016/j.mtbio.2023.100689
Received 14 April 2023; Received in revised form 25 May 2023; Accepted 2 June 2023
Available online 13 June 2023

seemed that $ONOO^-$ was more meaningful than other ROS due to the sensitivity to the disorders and the association with vital pathological events [20,21]. However, tracking $ONOO^-$ in physiological and pathological events is hard due to the short half-life of about 10 ms [22]. This factor also agreed with the necessity of real-time and in situ monitoring. Thus, the requirement can be focused on the developing practical instrument.

In recent decades, fluorescent probes have attracted the attentions of the investigators due to the high selectivity and sensitivity, good biocompatibility as well as non-invasion capability [23]. The optimization of the fluorescent probes gradually allowed the dynamic imaging to suit the requirement of real-time and in situ [24–26]. In particular, for the detection of $ONOO^-$, many fluorescent probes have been reported [27–37]. They showed unique properties, and some of them could even achieve the *in vivo* imaging. For further application of in-depth imaging, the steadiness of the probe should be more strictly confirmed. In the monitoring of liver injury, several fluorescent probes achieved the imaging via detecting molecular indexes including glutathione (GSH) and H_2S [38,39]. Although there were several important reports on the accurate imaging of $ONOO^-$ in liver injury [16,40–42], and some of them was deeply applied in the specialized induced models, the necessity on visualizing both the formation and inhibition of drug-induced liver injury was still an emergency.

In this work, an activable fluorescent probe for $ONOO^-$, named **NOP**, was constructed for the accurate imaging in the processes of formation and inhibition of drug-induced liver injury (Fig. 1A). The probe exhibited good stability, wide pH adaption, high specificity and sensitivity in the monitoring of $ONOO^-$, thus was applied for building the connection between the $ONOO^-$ level and the liver injury. Herein, Acetaminophen (APAP), a typical drug, was selected to induce the liver injury [43–45]. By focusing on the drug-induced liver injury, specific models were studied to reflect both the pathogenesis and treatment procedures. The information in this work might be helpful for realizing the early diagnosis and screening potent treating candidates in drug-induced liver injury cases.

2. Experimental section

2.1. The limit of detection (LOD) of *NOP*

The emission spectrum of free **NOP** (10 μM, 1% DMSO) in 10 mM PBS buffer (pH 7.4) was tested for 30 times to confirm the background noise σ. The slope was obtained from the linear curve of **NOP** (10 μM) and $ONOO^-$ (0–10 μM). The detection limit was calculated according to formula (3σ/slope). $\lambda_{ex} = 580$ nm, slit width: dex = dem = 10 nm. LOD = 0.11 μM.

2.2. Cytotoxicity with CCK8 assay

The cytotoxicity of **NOP** was verified by CCK8 assay. HepG2 cells were seeded into 96-well plates (1×10^3 per well). After adherent, the cells were incubated with different concentrations of **NOP** (0, 5, 10, 15, 20, 25, 30, 35, 40, 45 μM) for another 24 h in Normal culture environment. The 0 μM group was the equivalent volume DMSO-treated HepG2 cells. Then, CCK8 solution (10 μL per well) was added, then incubated for another 4 h. The prepared 96-well plate samples were detected by ELISA reader (ELx800, BioTek, USA) at 450 nm. Shaking the 96-well plate on the microplate reader for 5 min before testing. The experiments were repeated six times.

2.3. Liver tissue imaging and pathological examination

The intact liver tissue that was removed would be entrusted to the company (Wuhan Seville Biological Co., Ltd.) to cut into blank paraffin tissue sections of 4 μm for histopathological analysis. Thin sections (4 μm) were stained with H&E and Masson for histopathological study. Images of H&E and Masson stained sections were acquired by microscope (Olympus IX73) with 5× objective lens.

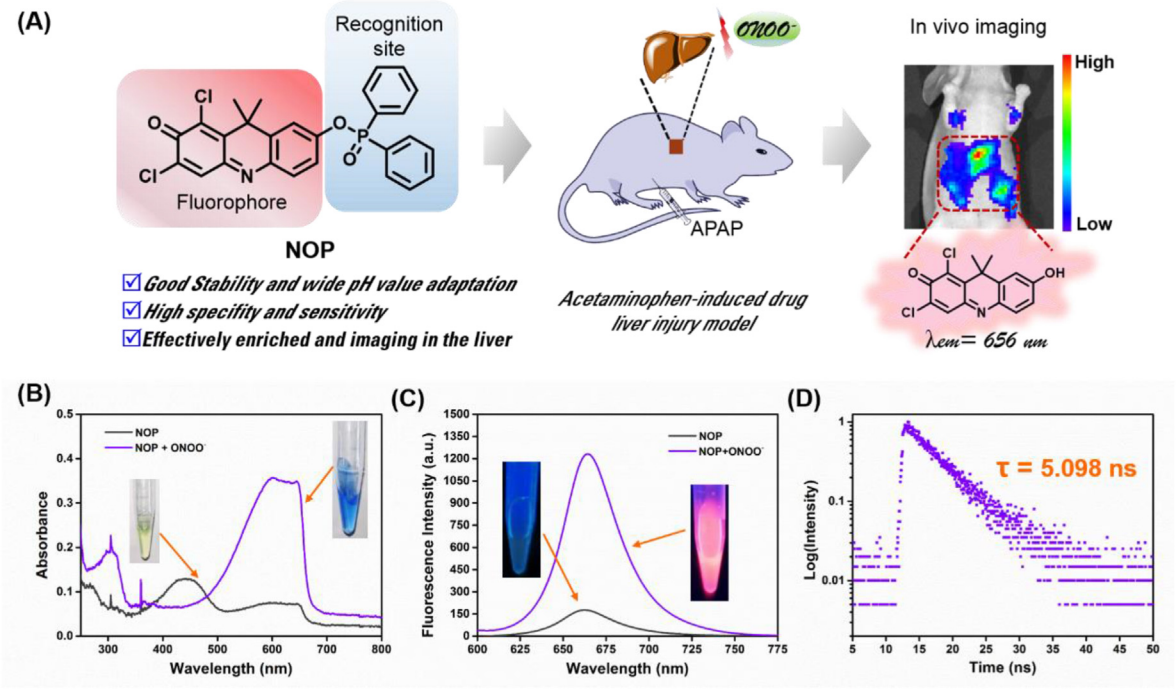

Fig. 1. (A) Schematic illustration of fluorescence probe, **NOP**, for real-time monitoring $ONOO^-$ fluctuation in drug-induced liver injury. (B) Ultraviolet absorption spectrum response of **NOP** to $ONOO^-$ for 5 min. Inset: The visual colors of probe **NOP** (10 μM) in the absence and presence of $ONOO^-$ (50 μM). (C) Fluorescence emission spectrum response of **NOP** to $ONOO^-$ for 5 min. Inset: The visual colors of probe **NOP** (10 μM) in the absence and presence of $ONOO^-$ (50 μM) under the UV lamp. (D) Fluorescence lifetime of **NOP**.

2.4. Detection of serum liver injury indexes

After all mice were induced by APAP, according to the method of animal model establishment (*1.7 Animal models and imaging*). Rapid extraction of blood from orbit with a capillary of 0.05 mm inner diameter. The collected serum samples were left standing at room temperature for 2 h, centrifuged at 3500 r/min for 15 min and collecting supernatant. The supernatant was re-centrifuged for 10 min at 3500 r/min. Serum liver injury indexes were detected using the ALT, ALP, AST, LDH, TBIL.

3. Results and discussion

3.1. Chemical synthesis and mechanism study

The synthetic route of the probe **NOP** was detailed in the Supporting Information. The fluorophore **DDAO** was prepared in two steps from *m*-hydroxybenzoic acid. Then the probe **NOP** was generated by reacting the quencher diphenylphosphinic chloride with the fluorophore in dichloromethane. The structures of the synthesized compounds were confirmed by satisfactory spectroscopic data including ^{1}H NMR, ^{13}C NMR, as well as HRMS in Supporting Information.

The response mechanism of **NOP** towards $ONOO^-$ was also preliminarily studied by analyzing the LC-MS spectra and HPLC (Figs. S1 and S2). The feature peaks of the fluorophore **DDAO** and the probe **NOP** were depicted in Figure S1a1, a2, b1 & b2, respectively. The LC-MS result of **NOP** solution after incubating with $ONOO^-$ in Figure S1c1 & c2 indicated the mechanism that $ONOO^-$ could cause the deprotection of the probe **NOP** to generate the original fluorophore **DDAO**.

3.2. Optical properties of the probe

Initially, the UV–vis and fluorescence spectra of the probe (10 μM) with the absence and presence of $ONOO^-$ (50 μM) were scanned (Fig. 1B and C). With the addition of $ONOO^-$, an obvious absorption peak appeared at about 600 nm, and from the naked eye the colorless system became blue (Fig. 1B). Meanwhile, with the addition of $ONOO^-$, there was a remarkable enhancement in fluorescence intensity at 656 nm under the excitation of 580 nm, and the non-fluorescent system exhibited a red fluorescence (Fig. 1C). The fluorescence lifetime of **NOP** was calculated as 5.098 ns (Fig. 1D), while the fluorescence quantum yield (FQY) of **NOP** was determined as 0.38.

By adding increasing concentrations (0–60 μM) of $ONOO^-$ into the system containing **NOP** (10 μM), the standard curve was built to reflect the relation between the fluorescence intensity and the $ONOO^-$ concentration. The fluorescence signal enhanced along with the increase of $ONOO^-$ concentration, and reached the plateau with about 60 μM $ONOO^-$ (Fig. 2A). With the linear range of 0–10 μM (Fig. 2B), the limit of detection (LOD) of **NOP** was calculated as 0.11 μM (from 3σ/slope). The probe here was highly sensitive to $ONOO^-$ among the reported data (Table S1). In both time and dose scale, the intensity of the detecting system containing **NOP** was positively correlated with the $ONOO^-$ concentration (Fig. 2C). Meanwhile, the fluorescence intensity of the response towards ONOO- was stable for over 48 h (Fig. S3). Subsequently, the selectivity and anti-interference of the detection were checked. Among a variety of competing species including cations, anions, amino acids, ROS and RNS, **NOP** only exhibited obvious fluorescence response towards $ONOO^-$, while the fluorescence signal was almost steady in the co-existence system containing both $ONOO^-$ and other species (Fig. 2D). To distinguish $ONOO^-$ from other ROS, both the recognition group and the response time herein ensured the selectivity. For the pH condition, the probe itself showed weak fluorescence within the tested range of 3.0–12.0, while the fluorescence intensity of the detecting system was steady within the range of 7.0–12.0 (Fig. 2E). The fluorescence intensity of the released fluorophore was affected by the

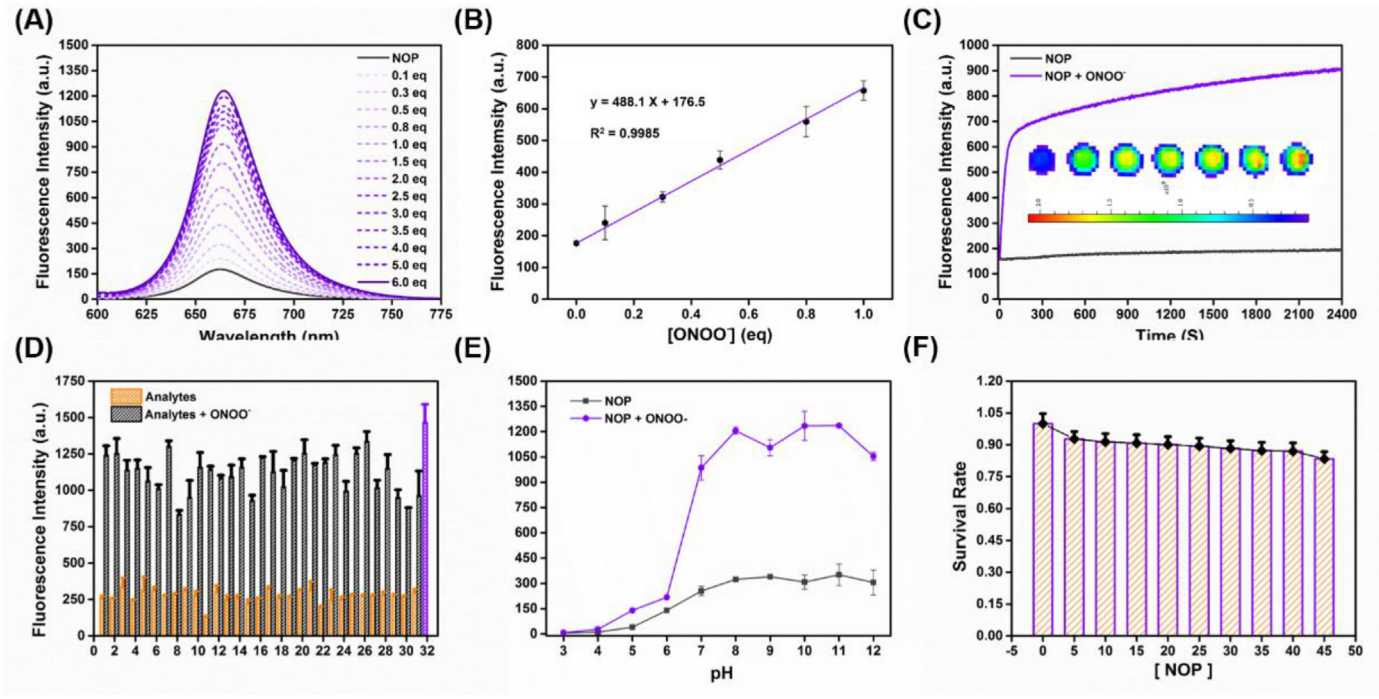

Fig. 2. (A) Fluorescence spectra of 10 μM **NOP** and 0–60 μM $ONOO^-$ for 5 min. (B) The linear relationship between **NOP** (10 μM) and $ONOO^-$ (from 0 to 10 μM). (C) Time-scan of fluorescence intensities of NOP with $ONOO^-$ (50 μM). Inset: Fluorescence images of **NOP** (10 μM) responded with different concentrations of $ONOO^-$ (0, 10, 20, 30, 40, 50, 60 μM). (D) Fluorescence intensity at 656 nm responses of **NOP** to various biological species for 5 min, including 1–9. Positive ion (100 μM Al^{3+}, Ca^{2+}, Cu^{2+}, Fe^{2+}, Fe^{3+}, K^+, Mg^{2+}, Na^+, Zn^{2+}), 10–17. Anion (100 μM AcO^-, Cl^-, ClO_4^-, CO_3^{2-}, HSO_3^-, $S_2O_3^{2-}$, SO_3^{2-}, SO_4^{2-}), 18–22. Amino acid (1 mM GSH, 100 μM Hcy, 100 μM Met, 100 μM Ser, 100 μM Cys), 23–27 (ROS species: 100 μM H_2O_2, •OH, $^1O_2^-$•, O_2^-, ClO^-), 28, 29 (RNS: 100 μM NO_2^-), 30, 31 (Others 100 μM N_2H_4, S^{2-}), 32 (50 μM $ONOO^-$). (E) Fluorescence intensity of 10 μM **NOP** reacted with or without $ONOO^-$ in various pH for 5 min. (F) Cell viability of HCT116 cells treated with **NOP** (0, 5, 10, 15, 20, 25, 30, 35, 40, 45 μM).

keto-enol isomerism, thus the increase of pH resulted in the preference of keto-form and the increase of fluorescence intensity [46,47]. Further tests were conducted to determine the photo-stability of the fluorophore, fluorescent probe and the reaction system. As shown in Fig. S4, after the irradiation with a laser at 580 nm for 30 min, the fluorescence intensity at 656 nm of each group kept stable. Accordingly, the probe **NOP** indicated stead performances in the monitoring of $ONOO^-$ in solution.

3.3. Intracellular imaging

In the topic of drug-induced liver injury, HepG2 (human hepatoellular carcinoma cell line) was chosen to conduct the intracellular imaging. Initially, the cototoxicity was evaluated with CCK8 assay. With 45 μM of **NOP**, the survival rate of HepG2 cells was still over 90% (Fig. 2F). This result indicated the low cototoxicity of **NOP**. Subsequently, the probe **NOP** was applied to imaging the exogenous $ONOO^-$ level in living HepG2 cells. Hoechst 33,342 dye was used to show the position of nucleus. As the extending of the incubation time with **NOP** (10 μM), the fluorescnece signal in the red channel enhanced and almost became stable within 30 min (Fig. S5). Then, when the incubation time was fixed as 30 min, **NOP** (10 μM) was used to imaging various concentrations of $ONOO^-$ (0–60 μM). As shown in Fig. 3A and B, the fluoresence signal in the red channel enhanced along with the increase of the $ONOO^-$ level, and almost reached the plateau when there was 60 μM $ONOO^-$. Afterwards, APAP was used to induce the endogenous $ONOO^-$ and **NOP** was used to imaging the dynamic of $ONOO^-$. After the addtion of 1 mM APAP, the fluorescence signal in the red channel gradually enhanced as the extending to incubation time, and it took about 8 h to reach the plateau (Fig. S6). To ensure the saturation of the fluorescence signal, we chose 12 h as the induction time of APAP. After the incubation with various concentration of APAP (0–1 mM) for 12 h, the fluorescence signal in the red channel indicated a dose-dependent enhancement (Fig. 3C and D). Moreover, after the incubation with 1 mM APAP for 8 h, Glu (1 mM, 12 h), GSH (1 mM, 12 h) and NAC (1 mM, 12 h) were used for a further incubation of 12 h separately. In the followed imaging by **NOP**, the fluorescence signal in the red channel decreased from the high intenity of the APAP-induced group (Fig. S7). This result agreed with the fact that these agents could consume $ONOO^-$ to pretect the liver cells [48,49].

3.4. Imaging in APAP-induced liver injury

Preliminarily, we checked whether **NOP** could achieve the *in vivo* imaging of $ONOO^-$. First of all by H&E staining of slices of major organs (eg., heart, liver, spleen, lung, stomach, and kidneys) revealed that ODP has good biocompatibility for *in vivo* studies (Fig. S8). The probe **NOP** (100 μM) and $ONOO^-$ (500 μM) were intraperitoneally injected. During the imaging period of 60 min, the fluorescence signal gradually enhanced as the time extended (Fig. 4A and B). This result indicated that **NOP** could monitor the $ONOO^-$ level *in vivo*. In this section, the APAP-induced liver injury mouse model was constructed, and the probe **NOP** (100 μM) was applied to accurate imaging both the formation and inhibition via monitoring the dynamics of $ONOO^-$ level. Then induction by APAP was designed as an orthogonal experiment with the scales of imaging time (0.1–2 h) and APAP treating time (0–12 h). As shown in Fig. 4C and D, the fluorescence signal enhanced along with the increase of the APAP-

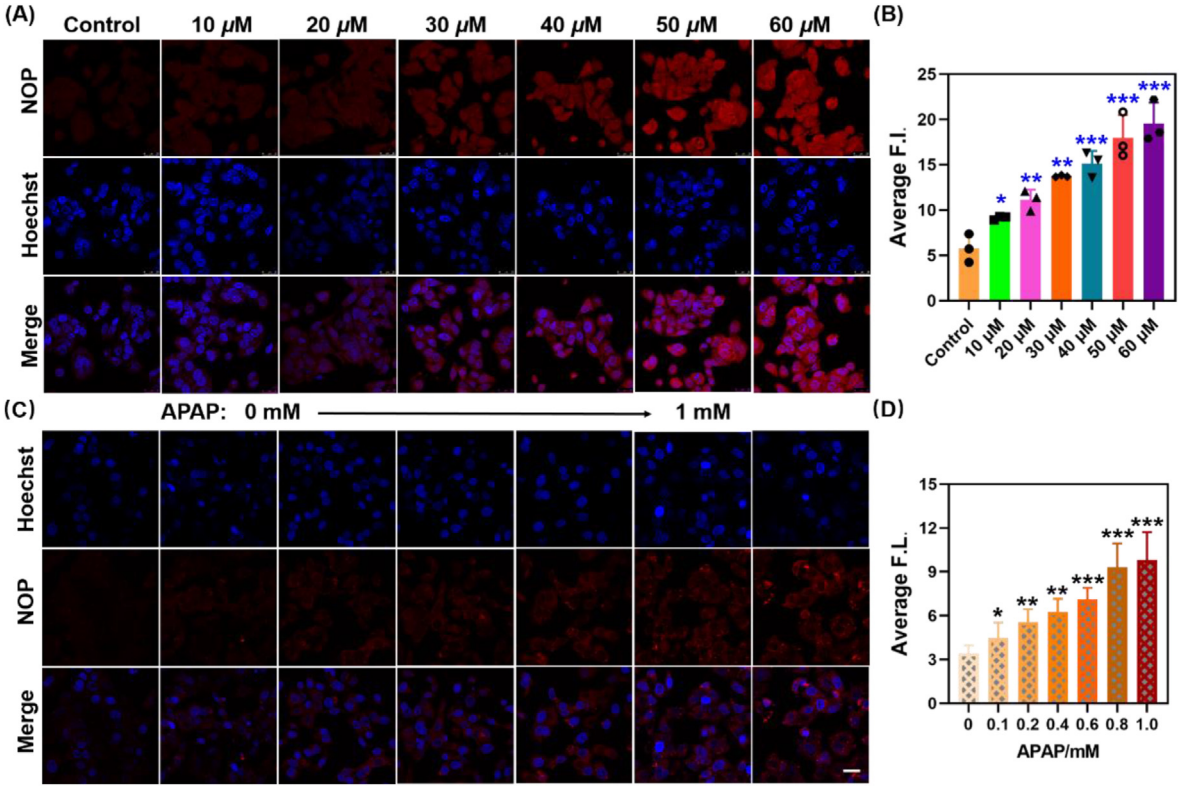

Fig. 3. Confocal fluorescence imaging of $ONOO^-$ in HepG2 cells. (A) Imaging of exogenous $ONOO^-$ in cells. The cells were pretreated with **NOP** (10 μM) for 15 min, then cells were incubated with 0, 10, 20, 30, 40, 50, 60 μM $ONOO^-$ for another 30min. Finally, commercial Hoechst 33,342 dye was added and stained for 15min. (B) Quantification of image data Fig. 3A. Data are presented as the average value, error bars were ±SD, n = 3. Statistical analysis was performed with one-way ANOVA with multiple comparisons. *p-value <0.05, **p-value <0.01, ***p-value <0.001. (C) HepG2 cells were coincubated with APAP (0, 0.1, 0.2, 0.4, 0.6, 0.8, 1.0 mM) for 12 h, then the cells were washed with PBS three times. After added the **NOP** (10 μM) for 30 min. Finally, commercial Hoechst 33,342 dye was added and stained for 15min. Images were collected on laser confocal with 60× objective lens. Hoechst 33,342 channel, λ_{ex} = 405 nm, λ_{em} = 415–485 nm; **NOP** channel, λ_{ex} = 580 nm, λ_{em} = 620–700 nm. Scale bar = 25 μM. (D) Quantification of image data Fig. 3C. Data are presented as the average value, error bars were ±SD, n = 3. Statistical analysis was performed with one-way ANOVA with multiple comparisons. *p-value <0.05, **p-value <0.01, ***p-value <0.001.

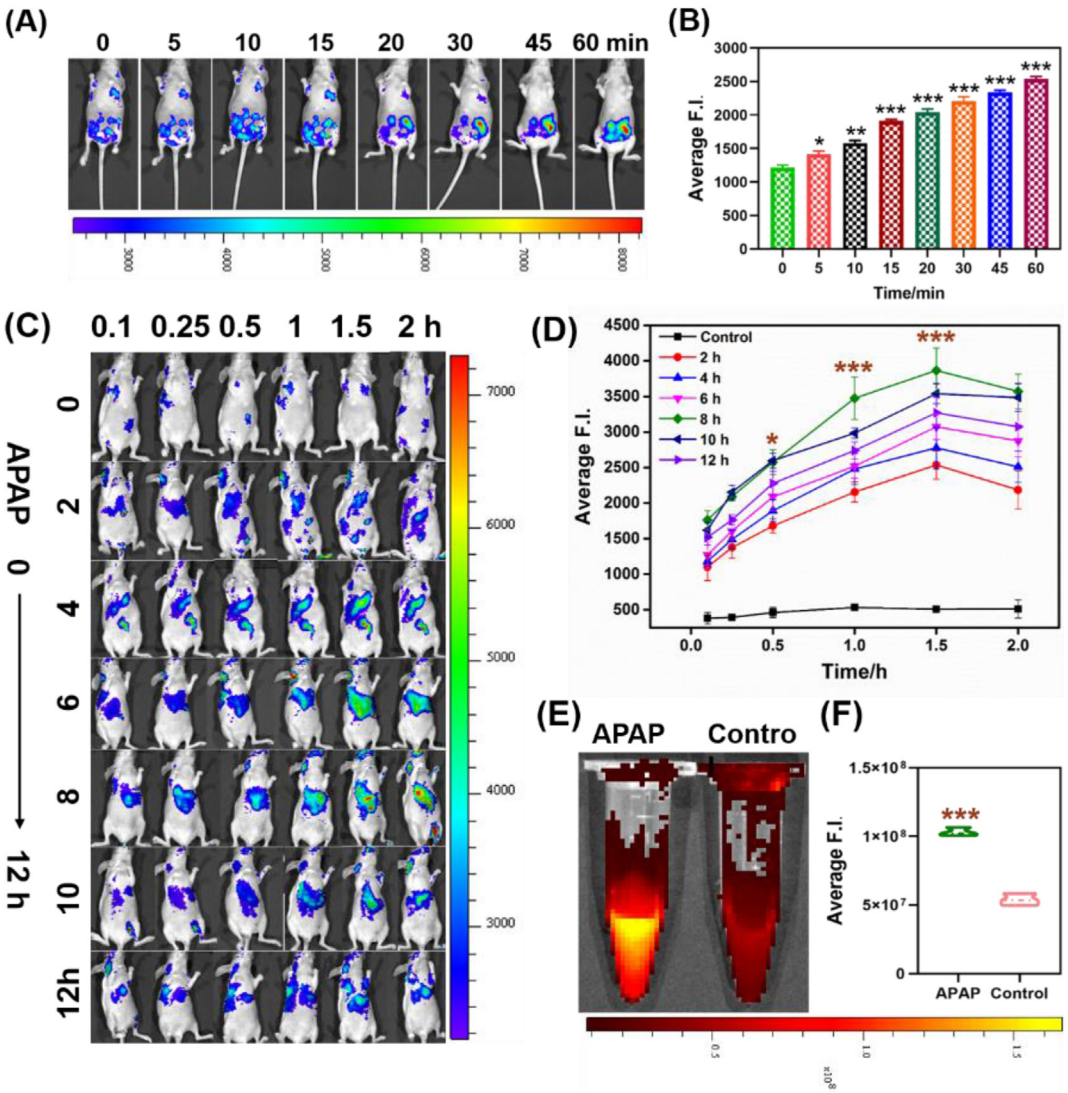

Fig. 4. In vivo imaging of $ONOO^-$ in mice. (A) The nude mice were intraperitoneal injection 100 μM **NOP** (200 μL in normal saline (NS)), and then intraperitoneal injected 500 μM $ONOO^-$ at the same location. After fluorescence images of mice were collected at different time point: 0, 5, 10, 15, 20, 30, 45, 60 min λ_{ex} = 560 nm, λ_{em} = 680 nm. (B) Quantification of image data Fig. 4A. Data are presented as the average value, error bars were ±SD, n = 3. Statistical analysis was performed with one-way ANOVA with multiple comparisons. *p-value <0.05, **p-value <0.01, ***p-value <0.001. (C) The nude mice were intraperitoneal injection 400 mg/kg APAP (200 μL in NS) for different time (0, 2, 4, 6, 8, 10, 12 h), and then via tail vein injection 100 μM **NOP** (200 μL in NS). After fluorescence images of mice were collected at different time point: 0.1, 0.25, 0.5, 1.0, 1.5, 2.0 h λ_{ex} = 580 nm, λ_{em} = 680 nm. (D) Quantification of image data Fig. 4C. Data are presented as the average value, error bars were ±SD, n = 3. Statistical analysis was performed with one-way ANOVA with multiple comparisons. *p-value <0.05, ***p-value <0.001. (E) Fluorescence image of representative collected urines of APAP drug-induced liver injury mode mice and WT mice. (F) Quantification of image data Fig. 4E. Data are presented as the average value, error bars were ±SD, n = 3. Statistical analysis was performed with one-way ANOVA with multiple comparisons. ***p-value <0.001.

induction time and the plateau was reached in 8 h; while longer imaging time also led to higher fluorescence signal, which reached the saturation within 1.5 h. Meanwhile, the collected urine samples of APAP-induced liver injury mode mice and WT mice were also tested by **NOP** (100 μM) for 24 h (Fig. 4E and F). As a result, the probe was excreted through the kidneys compared with the sample of WT mice, the urine sample of the APAP-induced liver injury mode mice exhibited obvious fluorescence signal.

On the other hand, the induction was designed as another orthogonal experiment with the scales of imaging time (0.1–2 h) and APAP dosages (0–500 mg/kg). As shown in Fig. 5A and B, the fluorescence signal enhanced along with the increase of the APAP concentration, and the plateau was reached when the concentration was 400 mg/kg. For the imaging time, the saturation was also reached within 1.5 h. Accordingly, in the APAP-induced models in both time scale and dose scale, the probe **NOP** could imaging the $ONOO^-$ dynamics. Afterwards, the liver injury in the above models was checked by pathological examination. As shown in Fig. S9 and Fig. S10, the fluorescence signal enhanced in time-dependent and dose-dependent manners under the induction of APAP. Therefore, by monitoring the fluorescence signal, the severity of the APAP-induced liver injury could be characterized. As shown in Fig. S11 and Fig. S12, the liver slice sections of the imaged model mice were compared with **NOP**-imaging, H&E and Masson staining. As the incubatuon time extended or the dosage increased, obvious color change and morphological injury could be observed in the staining sections. The severity of the injury reflected by the staining was consistent with the fluorescence enhancement of **NOP**-imaging in the red channel. In the separated liver tissues, the relative intensity of fluorescence signals was also consistent with that of the slice sections. For further ensuring the liver injury status of the APAP-induced models, the serum indexes including ALT, AST, ALP, TBIL and LDH were also tested (Fig. 5C and D & E). As the dosage of APAP increased, ALT, AST, ALP and LDH increased accordingly, while

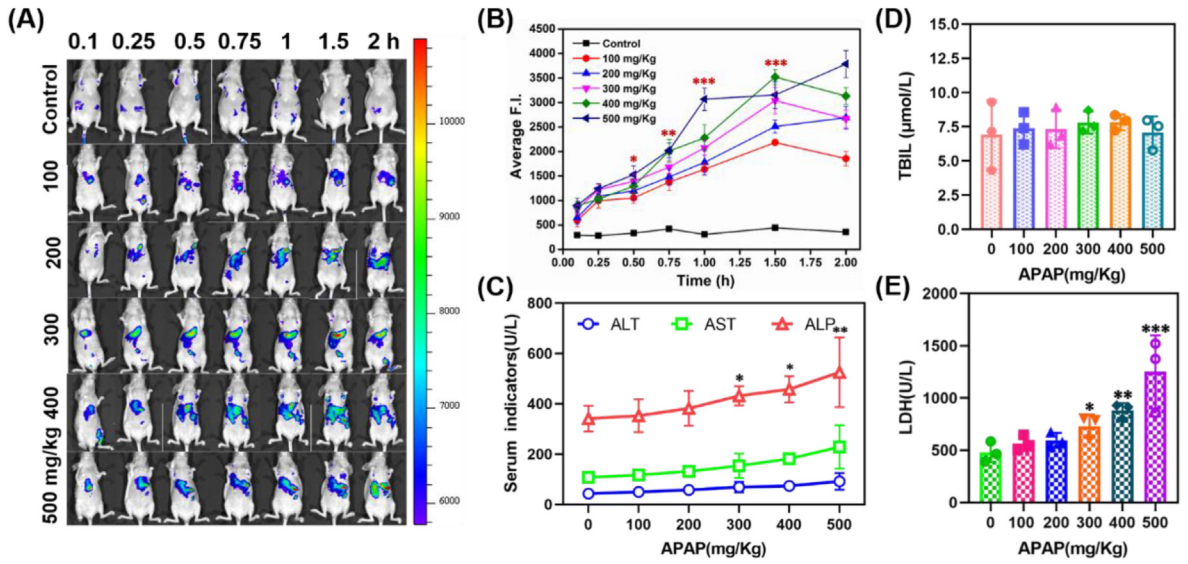

Fig. 5. (A)The Balb/c nude mice were intraperitoneal injection different concentration APAP: 0, 100, 200, 300, 400, 500 mg/kg APAP (200 μL in NS) for 8 h, and then via tail vein injection 100 μM **NOP** (200 μL in NS). After fluorescence images of mice were collected at different time point: 0.1, 0.25, 0.5, 0.75, 1, 1.5, 2.0 h $\lambda_{ex} = 580$ nm, $\lambda_{em} = 680$ nm. (B) Quantification of image data Fig. 5A. Data are presented as the average value, error bars were ±SD, n = 3. Statistical analysis was performed with one-way ANOVA with multiple comparisons. *p-value <0.05, ***p-value <0.001. (C) Serum liver injury indexes were measured. Serum liver injury marker ALT, AST, ALP was measured. n = 3, error bars were ±SD. Statistical analysis was performed with one-way ANOVA with multiple comparisons. *p-value <0.05, **p-value <0.01. (D & E) Serum liver injury marker TBIL and LDH was detected. Statistical analysis was performed with one-way ANOVA with multiple comparisons. n = 3, error bars were ±SD. *p-value <0.05, **p-value <0.01, ***p-value <0.001.

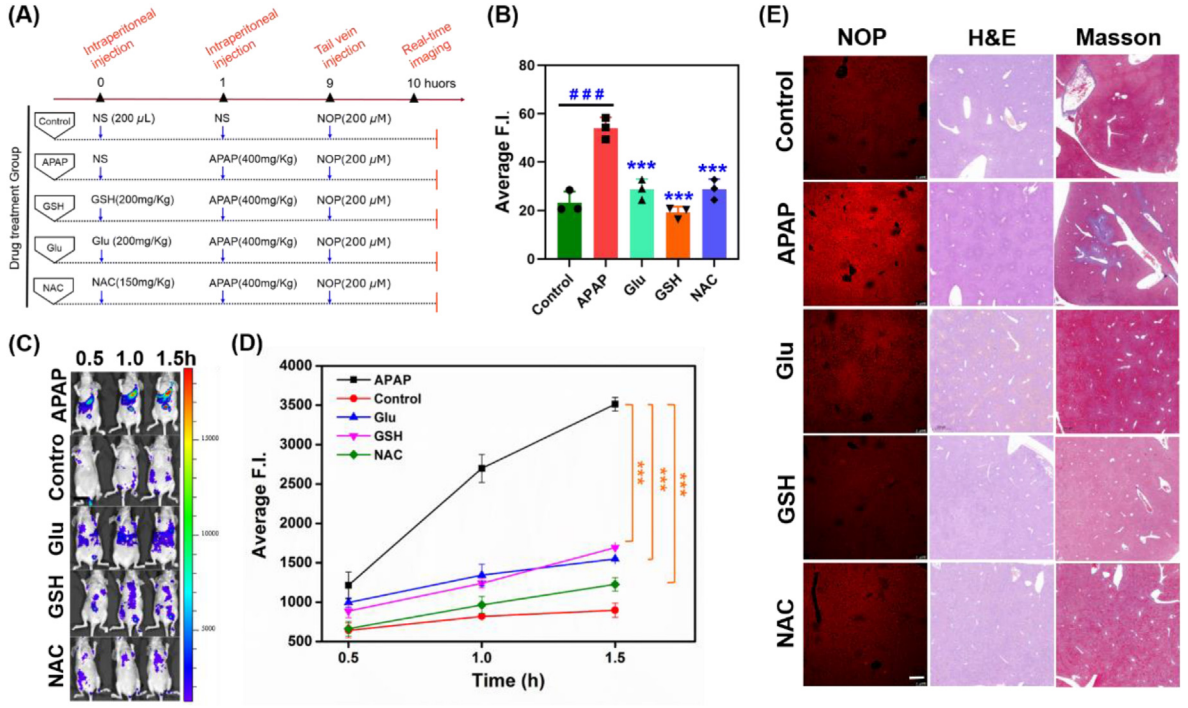

Fig. 6. Monitoring of the recovery of APAP drug-induced liver injury in mice upon NAC, Glu, GSH therapy. (A)Schematic diagram of the experimental design process. The nude mice were intraperitoneal injection 400 mg/kg APAP (200 μL in NS) for 8 h to induce liver injury, followed by intraperitoneal injected without or with GSH 200 mg/kg, NAC (150 mg/kg), Glu (200 mg/kg) for 12 h. And then via tail vein injection 100 μM **NOP** (200 μL in NS) into each mice. (C) The Fluorescence images were acquired at 0.5, 1.0, 1.5 h time point. $\lambda_{ex} = 580$ nm, $\lambda_{em} = 680$ nm. (D) Quantification of image data Fig. 6C. Data are presented as the average value, error bars were ±SD, n = 3. Statistical analysis was performed with one-way ANOVA with multiple comparisons. ***p-value <0.001. (E) Microscopy images of section of mice liver with different treatment. The liversection were stained with **NOP** (10 μM) for 15 min. Images were collected on laser confocal with 10× objective lens. $\lambda_{ex} = 580$ nm, $\lambda_{em} = 620$–700 nm. Scale bar = 100 μM. Histological H&E staining of liver sections after different treatments, Scale bar: 100 μm. Masson staining of liver sections for pathological examination, Scale bar: 100 μm. (B) Quantification of image data Fig. 6E on **NOP** fluorescence images. Data are presented as the average value, error bars were ±SD, n = 3. Statistical analysis was performed with one-way ANOVA with multiple comparisons. ### p-value <0.001, ***p-value <0.001.

TBIL stayed almost stable. In time scale (Fig. S13), the peak of the indexes including ALT, AST, ALP and LDH was at 8 h after the induction; while TBIL stayed almost stable. This result verified the injury status of the models. Additionally, after the comparison of the fluorescence signal intensity in different organs, we found that the difference between control group and APAP-induced group was significant in liver, while the difference in other organs was not obvious (Fig. S14).

After the imaging in the formation processes of APAP-induced liver injury, the inhibition process was also imaged in this work. The treating schedule was illustrated in Fig. 6A. The control group was incubated with the saline and imaged with **NOP** (100 μM). The APAP-induced group was treated with 400 mg/kg APAP, and finally imaged with **NOP** (100 μM). To construct the inhibition process, the inhibiting agents GSH (200 mg/kg), Glu (200 mg/kg) and NAC (150 mg/kg) was intraperitoneally injected before the injection of APAP. This kind of proposed inhibition was supported by the previous reports [50]. As shown in Fig. 6B & C, all the inhibiting agents could reduced the fluorescecne intensity increased by the APAP-induction. After the inhibition, the fluorescence intensity could be reduced to the level which was close to that of the control. In the time scale, during the 1.5 h imaging period, the result also indicated the significant inhibitory effect of the selected agents (Fig. 6D). By observing the fluorescence intensity of the isolated liver tissues, it can be seen that the tissues added with liver protection agent can effectively inhibit the liver damage caused by APAP (Fig. S15). After the confirmation of the fluorescence intensity by using the probe **NOP**, the connection between the injury severity and the fluorescence intensity was also checked. In Fig. 6E, we could find that, in the H&E and Masson staining sections, the color and morpological changes induced by APAP could be recovered by the treatment of inhibiting agents. The recovery effect was consistent with the reduction of the fluorescence intensity in the red channel. Accordingly, by using the probe **NOP**, the inhibition process of the APAP-induced liver injury could also be imaged, which might be helpful for screening potent treating candidates.

4. Conclusion

In summary, in this work, for the accurate imaging in the processes of formation and inhibition of drug-induced liver injury, an activable fluorescent probe for $ONOO^-$, named **NOP**, was developed. In the tests of general optical properties, the probe showed advantages including good stability, wide pH adaption, high specificity and sensitivity in the monitoring of $ONOO^-$. Based on the in-solution performance, the probe was further applied in the model mice. By using APAP as the inducer, the liver injury model was built. The construction of the liver injury model was confirmed by the pathological staining and the serum indexes including ALT, AST, ALP, TBIL as well as LDH. The fluorescence signal reflected by **NOP** was consistent with the results of pathological staining and the serum indexes tests. Monitored by **NOP** on the $ONOO^-$ dynamics, the formation of the drug-induced liver injury could be characterized with fluorescence enhancement in the red channel, while the inhibition by certain agents (GSH, Glu, NAC) led to the fluorescence reduction. Therefore, **NOP** could realize the early diagnosis of the drug-induced liver injury as well as the screening of potent treating candidates.

Credit author statement

Junming Dong: Methodology, Formal analysis, **Yushun Yang**: Data curation, Software, **Xiangjun Fan**: Tissue section experiment and Language polishing, **Hai-liang Zhu**: Writing – review & editing, Funding acquisition. **Zhen Li**: Conceptualization, Writing- Reviewing and Editing, Funding acquisition.

Declaration of competing interest

The authors declare that they have no known competing financial interests or personal relationships that could have appeared to influence the work reported in this paper.

Data availability

Data will be made available on request.

Acknowledgments

This research was supported by grants of Postdoctoral Science Foundation of China (No. 2019M651781 and 2019TQ0142), Nantong science and technology project (MS1202104) and the Innovation Fund for Technology of Nanjing University (2021).

Appendix A. Supplementary data

Supplementary data to this article can be found online at https://doi.org/10.1016/j.mtbio.2023.100689.

References

[1] C. Greenhill, Liver and adipose tissue control uridine biosynthesis, Nat. Rev. Endocrinol. 13 (5) (2017) 249, 249.
[2] N.M. Kettner, H. Voicu, M.J. Finegold, C. Coarfa, A. Sreekumar, N. Putluri, C.A. Katchy, C. Lee, D.D. Moore, L. Fu, Circadian homeostasis of liver metabolism suppresses hepatocarcinogenesis, Cancer Cell 30 (6) (2016) 909–924.
[3] H. Han, R. Desert, S. Das, Z. Song, D. Athavale, X. Ge, N. Nieto, Danger signals in liver injury and restoration of homeostasis, J. Hepatol. 73 (4) (2020) 933–951.
[4] H. Jaeschke, Preservation injury: mechanisms, prevention and consequences, J. Hepatol. 25 (5) (1996) 774–780.
[5] R. Loomba, S.L. Friedman, G.I. Shulman, Mechanisms and disease consequences of nonalcoholic fatty liver disease, Cell 184 (10) (2021) 2537–2564.
[6] J.H. Hoofnagle, E.S. Björnsson, Drug-induced liver injury—types and phenotypes, N. Engl. J. Med. 381 (3) (2019) 264–273.
[7] R.J. Andrade, N. Chalasani, E.S. Björnsson, A. Suzuki, G.A. Kullak-Ublick, P.B. Watkins, H. Devarbhavi, M. Merz, M.I. Lucena, N. Kaplowitz, Drug-induced liver injury, Nat. Rev. Dis. Prim. 5 (1) (2019) 1–22.
[8] G.A. Kullak-Ublick, R.J. Andrade, M. Merz, P. End, A. Benesic, A.L. Gerbes, G.P. Aithal, Drug-induced liver injury: recent advances in diagnosis and risk assessment, Gut 66 (6) (2017) 1154–1164.
[9] A.E. Rutherford, L.S. Hynan, C.B. Borges, D.G. Forcione, J.T. Blackard, W. Lin, A.R. Gorman, O.S. Shaikh, A. Reuben, E. Harrison, Serum apoptosis markers in acute liver failure: a pilot study, Clin. Gastroenterol. Hepatol. 5 (12) (2007) 1477–1483.
[10] Z. Jiang, D.-y. You, X.-c. Chen, J. Wu, Monitoring of serum markers for fibrosis during CCl4-induced liver damage: effects of anti-fibrotic agents, J. Hepatol. 16 (3) (1992) 282–289.
[11] M. Ushio-Fukai, D. Ash, S. Nagarkoti, E.J. Belin de Chantemele, D.J. Fulton, T. Fukai, Interplay between reactive oxygen/reactive nitrogen species and metabolism in vascular biology and disease, Antioxidants Redox Signal. 34 (16) (2021) 1319–1354.
[12] G. Vial, H. Dubouchaud, K. Couturier, C. Cottet-Rousselle, N. Taleux, A. Athias, A. Galinier, L. Casteilla, X.M. Leverve, Effects of a high-fat diet on energy metabolism and ROS production in rat liver, J. Hepatol. 54 (2) (2011) 348–356.
[13] A. LoGuidice, U.A. Boelsterli, Acetaminophen overdose-induced liver injury in mice is mediated by peroxynitrite independently of the cyclophilin D-regulated permeability transition, Hepatology 54 (3) (2011) 969–978.
[14] B. Kalyanaraman, Teaching the basics of redox biology to medical and graduate students: oxidants, antioxidants and disease mechanisms, Redox Biol. 1 (1) (2013) 244–257.
[15] L. Wu, J. Liu, X. Tian, R.R. Groleau, S.D. Bull, P. Li, B. Tang, T.D. James, Fluorescent probe for the imaging of superoxide and peroxynitrite during drug-induced liver injury, Chem. Sci. 12 (11) (2021) 3921–3928.
[16] C. Jin, P. Wu, Y. Yang, Z. He, H. Zhu, Z. Li, A novel fluorescent probe for the detection of peroxynitrite and its application in acute liver injury model, Redox Biol. 46 (2021), 102068.
[17] W. Zhang, J. Liu, P. Li, X. Wang, S. Bi, J. Zhang, W. Zhang, H. Wang, B. Tang, In situ and real-time imaging of superoxide anion and peroxynitrite elucidating arginase 1 nitration aggravating hepatic ischemia-reperfusion injury, Biomaterials 225 (2019), 119499.
[18] E.O. Hileman, J. Liu, M. Albitar, M.J. Keating, P. Huang, Intrinsic oxidative stress in cancer cells: a biochemical basis for therapeutic selectivity, Cancer Chemother. Pharmacol. 53 (2004) 209–219.
[19] M. Ye, Y. Han, J. Tang, Y. Piao, X. Liu, Z. Zhou, J. Gao, J. Rao, Y. Shen, A tumor-specific cascade amplification drug release nanoparticle for overcoming multidrug resistance in cancers, Adv. Mater. 29 (38) (2017), 1702342.
[20] P.C. Dedon, S.R. Tannenbaum, Reactive nitrogen species in the chemical biology of inflammation, Arch. Biochem. Biophys. 423 (1) (2004) 12–22.
[21] C. Fionda, M.P. Abruzzese, A. Santoni, M. Cippitelli, Immunoregulatory and effector activities of nitric oxide and reactive nitrogen species in cancer, Curr. Med. Chem. 23 (24) (2016) 2618–2636.

[22] R. Radi, G. Peluffo, M.a.N. Alvarez, M. Naviliat, A. Cayota, Unraveling peroxynitrite formation in biological systems, Free Radic. Biol. Med. 30 (5) (2001) 463–488.
[23] X. Liu, Y.-T. Chang, Fluorescent Probe Strategy for Live Cell Distinction, Chemical Society Reviews, 2022.
[24] M. Gao, F. Yu, C. Lv, J. Choo, L. Chen, Fluorescent chemical probes for accurate tumor diagnosis and targeting therapy, Chem. Soc. Rev. 46 (8) (2017) 2237–2271.
[25] S. Wang, W.X. Ren, J.-T. Hou, M. Won, J. An, X. Chen, J. Shu, J.S. Kim, Fluorescence Imaging of Pathophysiological Microenvironments, Chemical Society Reviews, 2021.
[26] S. Feng, J. Zheng, J. Zhang, Z. Gui, G. Feng, Fe2+ imaging in ferroptosis and drug-induced liver injury with a ratiometric near-infrared fluorescent probe, Sensor. Actuator. B Chem. 371 (2022), 132512.
[27] J. Miao, Y. Huo, Q. Liu, Z. Li, H. Shi, Y. Shi, W. Guo, A new class of fast-response and highly selective fluorescent probes for visualizing peroxynitrite in live cells, subcellular organelles, and kidney tissue of diabetic rats, Biomaterials 107 (2016) 33–43.
[28] P. Panizzi, M. Nahrendorf, M. Wildgruber, P. Waterman, J.-L. Figueiredo, E. Aikawa, J. McCarthy, R. Weissleder, S.A. Hilderbrand, Oxazine conjugated nanoparticle detects in vivo hypochlorous acid and peroxynitrite generation, J. Am. Chem. Soc. 131 (43) (2009) 15739–15744.
[29] T. Peng, N.-K. Wong, X. Chen, Y.-K. Chan, D.H.-H. Ho, Z. Sun, J.J. Hu, J. Shen, H. El-Nezami, D. Yang, Molecular imaging of peroxynitrite with HKGreen-4 in live cells and tissues, J. Am. Chem. Soc. 136 (33) (2014) 11728–11734.
[30] Y. Deng, G. Feng, Visualization of ONOO–and viscosity in drug-induced hepatotoxicity with different fluorescence signals by a sensitive fluorescent probe, Anal. Chem. 92 (21) (2020) 14667–14675.
[31] A.C. Sedgwick, H.-H. Han, J.E. Gardiner, S.D. Bull, X.-P. He, T.D. James, The development of a novel AND logic based fluorescence probe for the detection of peroxynitrite and GSH, Chem. Sci. 9 (15) (2018) 3672–3676.
[32] Z. Wang, W. Wang, P. Wang, X. Song, Z. Mao, Z. Liu, Highly sensitive near-infrared imaging of peroxynitrite fluxes in inflammation progress, Anal. Chem. 93 (5) (2021) 3035–3041.
[33] Y. Liu, Y. Ma, W. Lin, Construction of a bi-functional ratiometric fluorescent probe for detection of endoplasmic reticulum viscosity and ONOO-in cells and zebrafish, Sensor. Actuator. B Chem. 373 (2022), 132742.
[34] T. Huang, S. Yan, Y. Yu, Y. Xue, Y. Yu, C. Han, Dual-responsive ratiometric fluorescent probe for hypochlorite and peroxynitrite detection and imaging in vitro and in vivo, Anal. Chem. 94 (2) (2022) 1415–1424.
[35] X. Luo, Z. Cheng, R. Wang, F. Yu, Indication of dynamic peroxynitrite fluctuations in the rat epilepsy model with a near-infrared two-photon fluorescent probe, Anal. Chem. 93 (4) (2021) 2490–2499.
[36] J. Zhang, X. Zhen, J. Zeng, K. Pu, A dual-modal molecular probe for near-infrared fluorescence and photoacoustic imaging of peroxynitrite, Anal. Chem. 90 (15) (2018) 9301–9307.
[37] Y. Liu, S. Feng, S. Gong, G. Feng, Dual-Channel fluorescent probe for detecting viscosity and ONOO(-) without signal crosstalk in nonalcoholic fatty liver, Anal. Chem. 94 (50) (2022) 17439–17447.
[38] C. Zhang, Z. Qiu, L. Zhang, S. Wang, S. Zhao, Q. Pang, H. Liang, Mitochondria-targeted fluorescence/photoacoustic dual-modality imaging probe tailored for visual precise diagnosis of drug-induced liver injury, Anal. Chem. 94 (16) (2022) 6251–6260.
[39] L. Sun, J. Ouyang, Y. Ma, Z. Zeng, C. Zeng, F. Zeng, S. Wu, An activatable probe with aggregation-induced emission for detecting and imaging herbal medicine induced liver injury with optoacoustic imaging and NIR-II fluorescence imaging, Advanced Healthcare Materials 10 (24) (2021), 2100867.
[40] D. Cheng, J. Peng, Y. Lv, D. Su, D. Liu, M. Chen, L. Yuan, X. Zhang, De novo design of chemical stability near-infrared molecular probes for high-fidelity hepatotoxicity evaluation in vivo, J. Am. Chem. Soc. 141 (15) (2019) 6352–6361.
[41] X. Liu, L. He, X. Gong, Y. Yang, D. Cheng, J. Peng, L. Wang, X.-B. Zhang, L. Yuan, Engineering of reversible luminescent probes for real-time intravital imaging of liver injury and repair, CCS Chemistry 4 (1) (2022) 356–368.
[42] L. He, L.H. He, S. Xu, T.B. Ren, X.X. Zhang, Z.J. Qin, X.B. Zhang, L. Yuan, Engineering of reversible NIR-II redox-responsive fluorescent probes for imaging of inflammation in vivo, Angew. Chem. 134 (46) (2022), e202211409.
[43] B.L. Woolbright, H. Jaeschke, Role of the inflammasome in acetaminophen-induced liver injury and acute liver failure, J. Hepatol. 66 (4) (2017) 836–848.
[44] R.J. Andrade, N. Chalasani, E.S. Bjornsson, A. Suzuki, G.A. Kullak-Ublick, P.B. Watkins, H. Devarbhavi, M. Merz, M.I. Lucena, N. Kaplowitz, G.P. Aithal, Drug-induced liver injury, Nat. Rev. Dis. Prim. 5 (1) (2019) 58.
[45] Drug-induced liver injury, Nat. Rev. Dis. Prim. 5 (1) (2019) 59.
[46] L. Feng, Z. Tian, M. Zhang, X. He, X. Tian, Z. Yu, X. Ma, C. Wang, Real-time identification of gut microbiota with aminopeptidase N using an activable NIR fluorescent probe, Chin. Chem. Lett. 32 (10) (2021) 3053–3056.
[47] M.G. Chiorazzo, H.M. Tunset, A.V. Popov, B. Johansen, S. Moestue, E.J. Delikatny, Detection and differentiation of breast cancer sub-types using a cPLA2α activatable fluorophore, Sci. Rep. 9 (1) (2019) 6122.
[48] İ.İ. Boşgelmez, G. Güvendik, N-acetyl-L-cysteine protects liver and kidney against chromium (VI)-induced oxidative stress in mice, Biol. Trace Elem. Res. 178 (1) (2017) 44–53.
[49] M.S. Moosa, G. Maartens, H. Gunter, S. Allie, M.F. Chughlay, M. Setshedi, S. Wasserman, D.F. Stead, N. Hickman, A. Stewart, A randomized controlled trial of intravenous N-acetylcysteine in the management of anti-tuberculosis drug–induced liver injury, Clin. Infect. Dis. 73 (9) (2021) e3377–e3383.
[50] A.L. Chiew, C. Gluud, J. Brok, N.A. Buckley, Interventions for paracetamol (acetaminophen) overdose, Cochrane Database Syst. Rev. 2 (2018).